ACS APPLIED ELECTRONIC MATERIALS

pubs.acs.org/acsaelm Article

Anisotropic Spin Distribution and Perpendicular Magnetic Anisotropy in a Layered Ferromagnetic Semiconductor $(Ba,K)(Zn,Mn)_2As_2$

Shoya Sakamoto,* Guoqiang Zhao, Goro Shibata, Zheng Deng, Kan Zhao, Xiancheng Wang, Yosuke Nonaka, Keisuke Ikeda, Zhendong Chi, Yuxuan Wan, Masahiro Suzuki, Tsuneharu Koide, Arata Tanaka, Sadamichi Maekawa, Yasutomo J. Uemura, Changqing Jin, and Atsushi Fujimori

Cite This: *ACS Appl. Electron. Mater.* 2021, 3, 789−794 Read Online

ACCESS | Metrics & More | Article Recommendations | Supporting Information

ABSTRACT: The perpendicular magnetic anisotropy of a layered ferromagnetic semiconductor $(Ba,K)(Zn,Mn)_2As_2$ is studied using angle-dependent X-ray magnetic circular dichroism (XMCD) measurements. The large magnetic anisotropy with an anisotropy field of 0.85 T is deduced by fitting the Stoner−Wohlfarth model to the magnetic-field-angle dependence of the projected magnetic moment. Transverse XMCD spectra highlight the anisotropic distribution of Mn 3d electrons, where the d_{xz} and d_{yz} orbitals are less populated than the d_{xy} state because of the D_{2d} splitting that arises from the elongated $MnAs_4$ tetrahedra. The magnetic anisotropy originates from the degeneracy lifting of p−d_{xz}, d_{yz} hybridized states at the Fermi level. Namely, spin−orbit coupling lifts their degeneracy and induces energy gain when spins align along the z direction. The present system offers another tuning knob to control magnetic anisotropy through atomic orbital engineering.

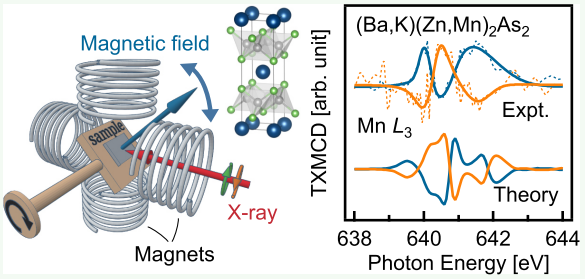

KEYWORDS: *ferromagnetic semiconductor, magnetic anisotropy, angle-dependent X-ray magnetic circular dichroism, spintronics, single crystal*

1. INTRODUCTION

Ferromagnetic semiconductors (FMSs) have attracted much attention since the discovery of ferromagnetism in (Ga,Mn)As and (In,Mn)As[1−4] as they are promising materials for future spintronics applications. Recently, a new FMS $Ba_{1-x}K_x(Zn_{1-y}Mn_y)_2As_2$ was synthesized in bulk form,[5,6] which crystallizes in the tetragonal $ThCr_2Si_2$ structure ($I4/mmm$) and is isostructural to 122-type Fe-based superconductors, as shown in Figure 1a. The host compound $BaZn_2As_2$ is a semiconductor with a narrow band gap of 0.2 eV.[7] In this system, one can independently control the numbers of carriers and spins by the heterovalent substitution of K^+ for Ba^{2+} and the isovalent substitution of Mn^{2+} for Zn^{2+}, respectively. Furthermore, with 30% K and 15% Mn substitution, the Curie temperature (T_C) reaches 230 K,[8] which is higher than T_C of (Ga,Mn)As, 200 K.[9] The transport and magnetic properties can also be controlled by external pressure.[10,11] The ferromagnetism is most likely carrier-induced as evidenced by previous experimental and theoretical studies.[5,10,12−16]

Because the crystal structure is inherently anisotropic, that is, the Ba ions are located between the quasi-two-dimensional (Zn/Mn)As layers and the $(Zn/Mn)As_4$ tetrahedra are elongated along the c-axis by ∼6% (see Figure 1a), sizable magnetic anisotropy would be expected. In fact, large perpendicular magnetic anisotropy, where the magnetic easy axis is along the c-axis, was observed by SQUID measurements.[6,17] Perpendicular magnetic anisotropy is useful for future magnetic memory applications because it can lead to a high bit density and reduce the critical current density for magnetization switching.[18] In general, magnetocrystalline anisotropy would not appear from the Mn^{2+} high-spin state ($^6A_1$) because of the lack of an orbital magnetic moment. In the case of (Ga,Mn)As, however, it was reported that biaxial strain from the substrate induces perpendicular or in-plane magnetic anisotropy.[19−23] This was ascribed to the orbital magnetic moment carried by the holes in the valence bands, which are magnetically coupled with the 3d electrons through p−d exchange interactions. In the case of $(Ba,K)(Zn,Mn)_2As_2$, however, the valence band top consists of only the As $4p_z$ orbital,[7] and the system does not have orbital degrees of

Received: October 23, 2020
Accepted: January 24, 2021
Published: February 4, 2021

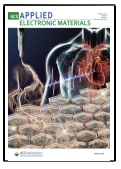

https://dx.doi.org/10.1021/acsaelm.0c00938
ACS Appl. Electron. Mater. 2021, 3, 789−794

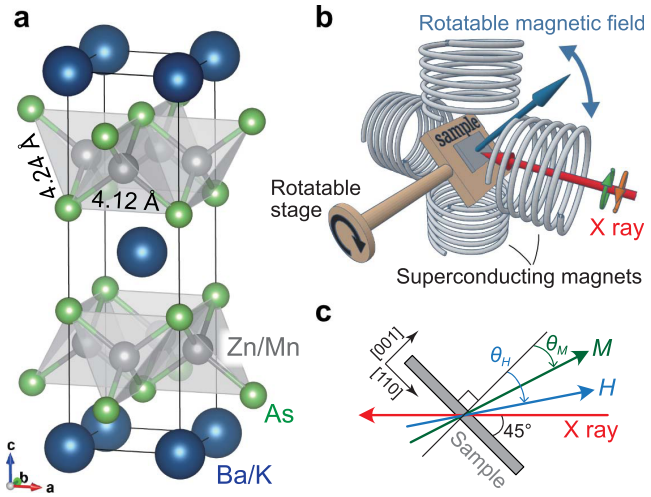

Figure 1. Crystal structure of $(Ba,K)(Zn,Mn)_2As_2$ and the experimental setup. (a) The unit cell of $(Ba,K)(Zn,Mn)_2As_2$. $(Zn/Mn)As_4$ tetrahedron elongated along the *c*-axis by ∼6%. The structures were drawn using VESTA.[28] (b) The schematic figure of the experimental apparatus. (c) Measurement geometry. The sample was placed so that the X-ray incident angle with respect to the sample surface was 45°. *H* and *M* denote the magnetic field and the magnetization, respectively, and θ_H (θ_M) denotes the angle of *H* (*M*) with respect to the sample normal.

freedom. Therefore, the orbital magnetic moment of holes alone in host valence bands cannot be responsible for the magnetic anisotropy of $(Ba,K)(Zn,Mn)_2As_2$.

X-ray magnetic circular dichroism (XMCD) is a powerful method to study magnetic anisotropy because one can directly probe the anisotropy of the spin (m_s) and orbital (m_l) magnetic moments. In addition, one can use angle-dependent XMCD (AD-XMCD) measurements to deduce the anisotropic spatial distribution of 3d spins, which appears as the magnetic dipole term (m_T) in the XMCD sum rule.[24] In particular, XMCD spectra taken under the transverse XMCD (TXMCD) geometry, where the applied magnetic field induces spin magnetic moments perpendicular to the incident X-ray, are known to be sensitive to the anisotropic distribution of 3d spins because the usually dominant spin contribution of the XMCD spectra vanishes. Note that there have been few experimental reports on the observation of TXMCD[25−27] because the direction of the magnetic field is usually fixed parallel to the incident X-rays in most XMCD measurement systems.

In the present study, we perform AD-XMCD measurements using our custom-designed apparatus and reveal that the large perpendicular magnetic anisotropy of $(Ba,K)(Zn,Mn)_2As_2$ originates from the degeneracy lifting of $p-d_{xz}$ and $p-d_{yz}$ hybridized orbitals due to spin−orbit interactions and the resulting energy gain when spins align along the *z*-direction.

2. METHODS

$Ba_{0.904}K_{0.096}(Zn_{0.805}Mn_{0.195})_2As_2$ single crystals with T_C = 60 K were grown by the flux technique (see the Supporting Information for the detail). AD-XMCD measurements were performed at BL-16A2 of the Photon Factory, KEK, where we installed our custom-designed apparatus[27,29] equipped with two pairs of superconducting magnets capable of applying magnetic fields up to 1 T that can be applied in any direction between the incident X-ray direction and a direction perpendicular to it (see Figure 1b for a schematic drawing). Prior to the measurements, we cleaved the samples *in situ* to obtain clean surfaces. Absorption signals were collected in a total electron yield mode. The measurement geometry is shown in Figure 1c. The sample was placed so that the angle between the incident X-ray and the [110] direction was 45°, at which the magnetic dipole-term contribution becomes the largest (see the Supporting Information for details). Because the direction of the incident X-rays was fixed in the present XMCD measurements, any artifact arising from the saturation effect[30] in the total electron yield mode was ruled out. XMCD spectra are obtained as the difference between two absorption spectra taken with right- and left-circularly polarized X-rays, while X-ray absorption spectroscopy (XAS) spectra are their summation.

To extract more information from the experimental XAS and XMCD spectra, we have performed CI cluster model calculations.[31] In the calculation, we assume a tetrahedral $[MnAs_4]^{-9}$ cluster (Mn^{3+} cluster). We adopt basically the same parameters as those used for (Ga,Mn)As[32] except that we add finite D_{2d} splitting so that the energy of the d_{xz} and d_{yz} orbitals lie higher in energy by 0.2 eV than the d_{xy} orbital, and the $d_{x^2-y^2}$ orbital is 0.2 eV higher than that of d_{z^2}. The parameters used for D_{2d} splitting are chosen based on the DFT calculations,[33] which shows a ∼0.2 eV splitting for the relevant orbitals (see the Supporting Information for further details).

3. RESULTS AND DISCUSSION

Figure 2a,b shows the XAS and XMCD spectra of $Ba_{0.904}K_{0.096}(Zn_{0.805}Mn_{0.195})_2As_2$ recorded at the Mn $L_{2,3}$ absorption edges. Here, the XMCD spectrum was taken with the magnetic field along the light direction and was dominated by the spin component. We thus refer to this spectrum as the

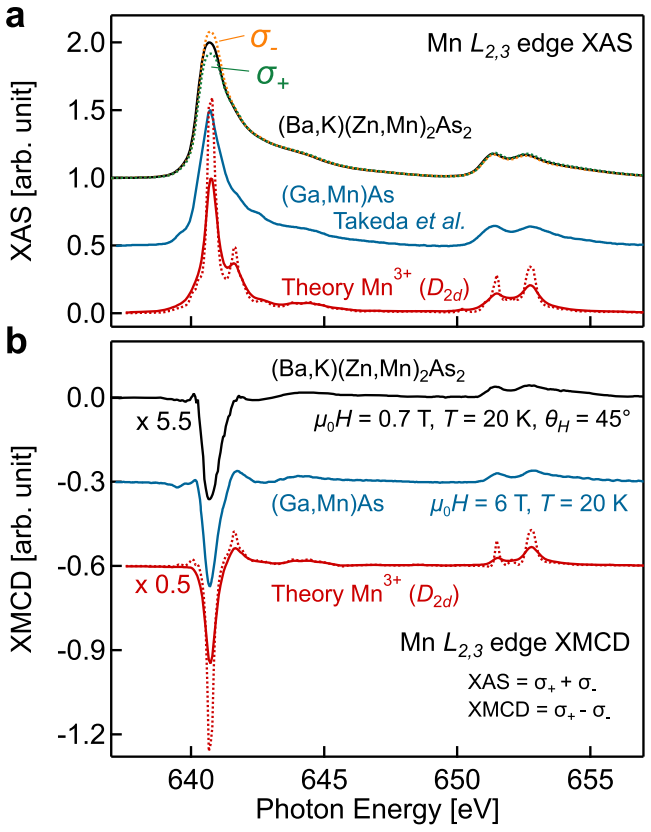

Figure 2. (a, b) Mn $L_{2,3}$-edge XAS and LXMCD spectra of $Ba_{0.904}K_{0.096}(Zn_{0.805}Mn_{0.195})_2As_2$ shown by black curves. The spectra of (Ga,Mn)As,[34] 2008 American Physical Society, and the cluster model calculation are also shown by blue and red dashed curves, respectively. The calculated spectra were broadened (red solid curves) using a Lorentzian function with an FWHM of 0.25 eV (0.4 eV) at the L_3 (L_2) edge.

https://dx.doi.org/10.1021/acsaelm.0c00938
ACS Appl. Electron. Mater. 2021, 3, 789−794

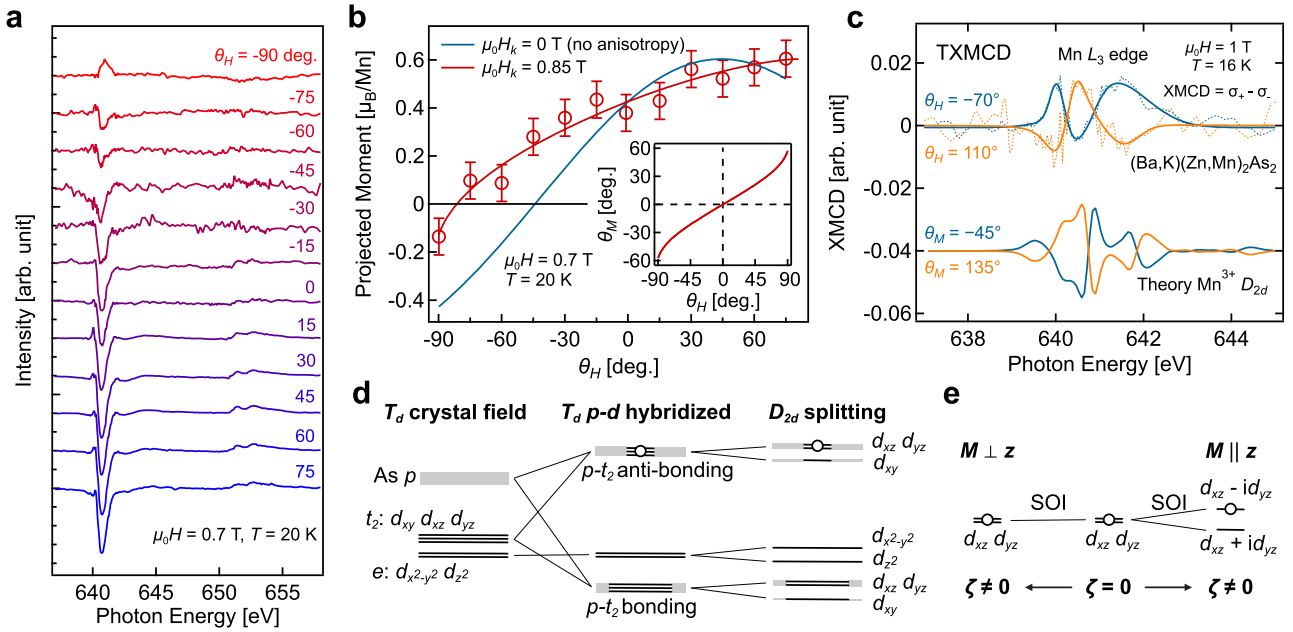

Figure 3. (a, b) Magnetic-field-angle dependence of the XMCD spectra and Mn magnetic moment projected onto the incident light direction. In panel (b), the solid curves represent the results of the simulation performed using the Stoner−Wohlfarth model, and the inset shows the simulated magnetic moment direction as a function of the magnetic field angle. (c) Transverse XMCD spectra measured with positive and negative transverse magnetic fields. The dashed curves at the top are the actual data, while the overlaid solid curves are guide to the eye, which are obtained by curve fitting with three Voigt functions. Calculated spectra are also shown at the bottom. (d) Schematic energy diagram of the occupied majority-spin Mn 3d orbitals in $(Ba,K)(Zn,Mn)_2As_2$. Here, white circles represent doped holes. (e) The schematic energy diagram of the top-most d_{xz} and d_{yz} levels with holes showing how the perpendicular magnetic anisotropy emerges as a result of the degeneracy lifting caused by spin−orbit interaction ζ.

longitudinal XMCD (LXMCD) spectrum hereafter. The XAS and LXMCD spectra exhibit multiplet features and are very similar to those of (Ga,Mn)As,[34,35] which are shown by the blue curves in Figure 2a,b. This indicates the localized nature of the Mn 3d electrons and is consistent with the carrier-induced ferromagnetism model, where itinerant holes mediate ferromagnetic interactions between the localized Mn spins. Here, the positive peak in the LXMCD spectrum at 642 eV located just above the dominant negative peak at 640 eV is smaller than that in the (Ga,Mn)As spectrum. This may reflect the difference in the electronic structures of (Ga,Mn)As and $(Ba,K)(Zn,Mn)_2As_2$.

The calculated spectra are shown by the red dashed curves in Figure 2a,b. The calculated spectra are broadened using a Lorentzian function with a full-width at half-maximum (FWHM) of 0.25 eV (0.4 eV) for the L_3 (L_2) edge to account for the core-hole lifetime.[36] The broadened spectra are shown by red solid curves, and they agree well with the experimental spectra. Note that the XMCD pre-edge peak around 640 eV is broadened out, and one may need to consider the final-state dependence of the core-hole lifetime[36] to reproduce both sharp pre-edge peak and the broad asymmetric main peak with a tail on the higher energy side.

Figure 3a shows XMCD spectra taken with various magnetic field angles. We deduce the total Mn magnetic moments projected onto the incident light direction using the XMCD sum rules. Here, we assume that the hole number is 5 and that the correction factor for the spin sum rule is 1.47.[35,37,38] Figure 3b shows thus deduced projected magnetic moments. If there was no magnetic anisotropy and magnetic moments always pointed toward the magnetic field direction, the data would follow a sine curve, as shown by the blue curve in Figure 3b. However, the data clearly deviate from the sine curve, indicating considerable magnetic anisotropy in this system. Here, we reproduce the data using the Stoner−Wohlfarth model. In this model, the total energy of the system is expressed as

$$E = -\mu_0 M_{sat} H \cos(\theta_M - \theta_H) + \frac{\mu_0}{2} M_{sat}^2 \cos^2\theta_M - K_U \cos^2\theta_M \quad (1)$$

where μ_0 denotes the permeability of the vacuum, M_{sat} is the saturation magnetization, H is the magnitude of the magnetic field, and K_U is the uniaxial magnetocrystalline anisotropy energy per unit volume. As shown in Figure 1c, θ_M and θ_H represent the angles of the magnetic moment and the magnetic field relative to the sample normal (c-axis direction), respectively. The first term represents the Zeeman energy, the second term represents the shape anisotropy energy, and the third term represents the uniaxial anisotropy energy. From this formula, one can calculate θ_M [or the projected moment $M_{sat}\cos(45° - \theta_M)$] for given θ_H, H, M_{sat}, and K_U values by minimizing the total energy E. In this way, we have fitted the data by treating K_U and M_{sat} as free parameters, and the results are shown by the red curve in Figure 3b. The fit yielded $K_U = (6.2 \pm 0.5) \times 10^4$ J/m^3 and saturation magnetization per Mn atom $m_{Mn} = 0.60 \pm 0.03\ \mu_B$. These values give an anisotropy field $\mu_0 H_K = 2K_U/M_{sat}$ of 0.85 ± 0.07 T. A positive value of K_U means that the easy axis is along the c-axis, which is consistent with a previous study.[17] The obtained m_{Mn} of 0.60 μ_B at 20 K is also consistent with a previous study's[6] saturation magnetization (not shown here) but significantly smaller than that of (Ga,Mn)As, 2−4 μ_B.[34,35] The cause of the reduction was theoretically attributed to the preferential formation of antiferromagnetically coupled nearest-neighbor Mn pairs[15] but should be clarified experimentally in future studies, for

https://dx.doi.org/10.1021/acsaelm.0c00938
ACS Appl. Electron. Mater. 2021, 3, 789−794

example, by performing XMCD measurements at various temperatures and magnetic fields.[38−40]

Figure 3c shows the TXMCD spectra, namely, XMCD spectra taken with the transverse geometry (θ_H = −70, 110° or θ_M ∼ −45, 135°) at which the spin component in the projected magnetic moment disappears and only the magnetic dipole term is present. For the numerical correspondence between θ_M and θ_H in the TXMCD geometry, refer to the inset of Figure 3b. The angles of the magnetic field were set such that the XMCD intensity was minimized. In Figure 3c, the dashed curves represent the actual data and solid curves are guide to the eye, which are obtained by curve fitting with three Voigt functions. The spectral line shape is very different from that of LXMCD, indicating that the signals observed here are not due to the residual spin component. Moreover, the sign of the TXMCD spectra is reversed by rotating the magnetic field by 180°. If these weak TXMCD spectra were just differential XAS spectra resulting from the slight photon energy difference between left- and right-circularly polarized X-rays, the two TXMCD spectra taken with the different magnetic field directions should coincide. Therefore, the sign reversal observed here is strong evidence to prove that the TXMCD signals are not artifacts but are real.

The calculated TXMCD spectra are also shown at the bottom of Figure 3c. Although there are some discrepancies in the line shapes, the overall features capture the experimental observations well. According to the calculation, 0.2 eV D_{2d} splitting resulted in almost fully occupied (∼98% filled) majority-spin d_{xy}, d_{z^2}, and $d_{x^2-y^2}$ orbitals and slightly less occupied (∼89% filled) d_{xz} and d_{yz} orbitals. Therefore, holes are predominantly doped into the d_{xz} and d_{yz} orbitals or p−d_{xz} and p−d_{yz} hybridized orbitals. Note that the minority-spin orbitals are almost completely empty.

This situation is schematically depicted in Figure 3d. Under the tetrahedral crystal field, the five Mn 3d orbitals are split into doubly degenerate e ($d_{x^2-y^2}$, d_{z^2}) orbitals and triply degenerate t_2 (d_{xy}, d_{xz}, d_{yz}) orbitals, as shown on the left-hand side of Figure 3d. The t_2 orbitals strongly hybridize with As 4p orbitals and form bonding and antibonding p−t_2 orbitals, while the e orbitals remain intact, as shown in the middle column of Figure 3d. The bonding and antibonding p−t_2 hybridized orbitals predominantly consist of t_2 and p orbitals, respectively. This orbital configuration is realized in cubic (Ga,Mn)As, and the holes residing in the antibonding p−t_2 hybridized states are the source of ferromagnetic exchange interactions. The elongation or compression of the $MnAs_4$ tetrahedra along the c-axis splits each of the t_2 and e energy levels further into sublevels: the t_2 level splits into (d_{xz}, d_{yz}) and d_{xy} levels, and the e level splits into $d_{x^2-y^2}$ and d_{z^2} levels. In the present system, the d_{xz} and d_{yz} levels are higher in energy than the d_{xy} level, and the $d_{x^2-y^2}$ level is higher in energy than the d_{z^2} level,[33] as shown on the right-hand side of Figure 3d. The doped holes thus reside in the p−d_{xz} and p−d_{yz} hybridized antibonding orbitals.

Magnetocrystalline anisotropy arises as a consequence of the energy gain of electrons occupying crystal-field-split orbitals caused by spin−orbit coupling when spins are aligned along a certain crystallographic direction, and only the orbitals near the Fermi level are relevant. In the present system, the p−d_{xz} and p−d_{yz} hybridized antibonding orbitals near the Fermi level with holes in them should be responsible for the magnetic anisotropy. Figure 3e shows how the partially occupied d_{xz} and d_{yz} orbitals can give rise to perpendicular (z-axis) magnetic anisotropy. When spins are aligned along the z-axis by a magnetic field, the degeneracy of the d_{xz} and d_{yz} orbitals will be lifted due to spin−orbit interactions to form $d_{xz} \pm id_{yz}$ (L_z = ±1) orbitals, resulting in an energy gain. On the other hand, when spins are aligned in the x−y plane, the d_{xz} and d_{yz} orbitals remain degenerate because any linear combination of these orbitals cannot form the eigenstate of L_x or L_y, and thus, there is no energy gain. This anisotropy of the orbital magnetic moment may explain the difference in the out-of-plane and in-plane saturation magnetizations observed in a previous study.[6] This situation is similar to the cases of Fe/MgO[41,42] and Co/Pt interfaces,[43] where the origin of their large perpendicular magnetic anisotropy was attributed to the degeneracy lifting of the d_{xz} and d_{yz} orbitals near the Fermi level.

The present results also suggest that it is possible to control the magnetic anisotropy by changing the number of carriers to change the electron occupation of each d orbital or even by isoelectric substitutions that change the magnitude of the D_{2d} splitting. These degrees of freedom, tuned by charge carrier engineering and atomic orbital engineering, would enable one to independently control the Curie temperature, carrier concentration, and magnetic anisotropy, which would be useful for future spintronics applications.

4. CONCLUSIONS

In summary, we performed an angle-dependent XMCD study to reveal the origin of the perpendicular magnetic anisotropy of $(Ba,K)(Zn,Mn)_2As_2$. Using the Stoner−Wohlfarth model, the magnetic anisotropy energy was estimated to be $K_U = (6.2 \pm 0.5) \times 10^4$ J/m^3, and the saturation magnetization per Mn atom was estimated to be $m_{Mn} = 0.60 \pm 0.03\ \mu_B$. We observed transverse XMCD spectra, which were well reproduced by performing cluster-model calculations with D_{2d} splitting where holes reside in the d_{xz} and d_{yz} orbitals. We conclude that the magnetic anisotropy originates from the degeneracy lifting of those orbitals due to spin−orbit coupling and the resulting energy gain when spins are aligned along the z-direction.

■ ASSOCIATED CONTENT

Supporting Information

The Supporting Information is available free of charge at https://pubs.acs.org/doi/10.1021/acsaelm.0c00938.

Details of sample growth; magnetic dipole term; the cluster model calculations; and calculations with various D_{2d} splitting parameters (PDF)

■ AUTHOR INFORMATION

Corresponding Author

Shoya Sakamoto − *Department of Physics and The Institute for Solid State Physics, The University of Tokyo, Tokyo 113-0033, Japan*; orcid.org/0000-0002-2405-1465; Email: shoya.sakamoto@issp.u-tokyo.ac.jp

Authors

Guoqiang Zhao − *Beijing National Laboratory for Condensed Matter Physics, Institute of Physics, Chinese Academy of Sciences, Beijing 100190, China*

Goro Shibata − *Department of Physics, The University of Tokyo, Tokyo 113-0033, Japan*

Zheng Deng − *Beijing National Laboratory for Condensed Matter Physics, Institute of Physics, Chinese Academy of Sciences, Beijing 100190, China*

https://dx.doi.org/10.1021/acsaelm.0c00938
ACS Appl. Electron. Mater. 2021, 3, 789−794

Kan Zhao − *Beijing National Laboratory for Condensed Matter Physics, Institute of Physics, Chinese Academy of Sciences, Beijing 100190, China*
Xiancheng Wang − *Beijing National Laboratory for Condensed Matter Physics, Institute of Physics, Chinese Academy of Sciences, Beijing 100190, China*
Yosuke Nonaka − *Department of Physics, The University of Tokyo, Tokyo 113-0033, Japan*
Keisuke Ikeda − *Department of Physics, The University of Tokyo, Tokyo 113-0033, Japan*
Zhendong Chi − *Department of Physics, The University of Tokyo, Tokyo 113-0033, Japan*
Yuxuan Wan − *Department of Physics, The University of Tokyo, Tokyo 113-0033, Japan*
Masahiro Suzuki − *Department of Physics, The University of Tokyo, Tokyo 113-0033, Japan*
Tsuneharu Koide − *Photon Factory, Institute of Materials Structure Science, High Energy Accelerator Research Organization (KEK), Tsukuba, Ibaraki 305-0801, Japan*
Arata Tanaka − *Department of Quantum Matter, Graduate School of Advanced Sciences of Matter (ADSM), Hiroshima University, Higashi-Hiroshima 739-8530, Japan*
Sadamichi Maekawa − *RIKEN Center for Emergent Matter Science (CEMS), Saitama 351-0198, Japan; Kavli Institute for Theoretical Sciences, University of Chinese Academy of Sciences, Beijing 100190, China*
Yasutomo J. Uemura − *Department of Physics, Columbia University, New York 10027, United States*
Changqing Jin − *Beijing National Laboratory for Condensed Matter Physics, Institute of Physics, Chinese Academy of Sciences, Beijing 100190, China*
Atsushi Fujimori − *Department of Physics, The University of Tokyo, Tokyo 113-0033, Japan; Department of Applied Physics, Waseda University, Tokyo 169-8555, Japan*

Complete contact information is available at: https://pubs.acs.org/10.1021/acsaelm.0c00938

Notes

The authors declare no competing financial interest.

■ ACKNOWLEDGMENTS

The authors thank Kenta Amemiya and Masako Sakamaki for their valuable technical support at the Photon Factory, KEK. This work was supported by the Grants-in-Aid for Scientific Research from the JSPS (Grants Nos. 15H02109, 15K17696, and 19K03741). The experiment was performed under the approval of the Program Advisory Committee (Proposal No. 2016S2-005, 2016G066). The work at IOPCAS was supported by the NSF & MOST of China through research projects. The work at Columbia was supported by the US NSF DMR1610633. S.S. acknowledges financial support from the Advanced Leading Graduate Course for Photon Science (ALPS) and the JSPS Research Fellowship for Young Scientists. A.F. acknowledges support as an adjunct member of the Center for Spintronics Research Network (CSRN), the University of Tokyo under the Spintronics Research Network of Japan (Spin-RNJ).

■ REFERENCES

(1) Ohno, H. Making Nonmagnetic Semiconductors Ferromagnetic. *Science* **1998**, *281*, 951−956.
(2) Munekata, H.; Ohno, H.; von Molnar, S.; Segmüller, A.; Chang, L. L.; Esaki, L. Diluted magnetic III-V semiconductors. *Phys. Rev. Lett.* **1989**, *63*, 1849−1852.
(3) Dietl, T.; Ohno, H. Dilute ferromagnetic semiconductors: Physics and spintronic structures. *Rev. Mod. Phys.* **2014**, *86*, 187−251.
(4) Jungwirth, T.; Wunderlich, J.; Novák, V.; Olejník, K.; Gallagher, B. L.; Campion, R. P.; Edmonds, K. W.; Rushforth, A. W.; Ferguson, A. J.; Němec, P. Spin-dependent phenomena and device concepts explored in (Ga,Mn)As. *Rev. Mod. Phys.* **2014**, *86*, 855−896.
(5) Zhao, K.; Deng, Z.; Wang, X. C.; Han, W.; Zhu, J. L.; Li, X.; Liu, Q. Q.; Yu, R. C.; Goko, T.; Frandsen, B.; Liu, L.; Ning, F.; Uemura, Y. J.; Dabkowska, H.; Luke, G.; Luetkens, H.; Morenzoni, E.; Dunsiger, S. R.; Senyshyn, A.; Böni, P.; Jin, C. Q. New diluted ferromagnetic semiconductor with Curie temperature up to 180 K and isostructural to the '122' iron-based superconductors. *Nat. Commun.* **2013**, *4*, No. 1442.
(6) Zhao, G. Q.; Lin, C. J.; Deng, Z.; Gu, G. X.; Yu, S.; Wang, X. C.; Gong, Z. Z.; Uemera, Y. J.; Li, Y. Q.; Jin, C. Q. Single Crystal Growth and Spin Polarization Measurements of Diluted Magnetic Semiconductor $(BaK)(ZnMn)_2As_2$. *Sci. Rep.* **2017**, *7*, No. 14473.
(7) Xiao, Z.; Ran, F.-Y.; Hiramatsu, H.; Matsuishi, S.; Hosono, H.; Kamiya, T. Epitaxial growth and electronic structure of a layered zinc pnictide semiconductor, β-$BaZn_2As_2$. *Thin Solid Films* **2014**, *559*, 100−104.
(8) Zhao, K.; Chen, B.; Zhao, G.; Yuan, Z.; Liu, Q.; Deng, Z.; Zhu, J.; Jin, C. Ferromagnetism at 230 K in $(Ba_{0.7}K_{0.3})(Zn_{0.85}Mn_{0.15})_2As_2$ diluted magnetic semiconductor. *Chin. Sci. Bull.* **2014**, *59*, 2524−2527.
(9) Chen, L.; Yang, X.; Yang, F.; Zhao, J.; Misuraca, J.; Xiong, P.; von Molnár, S. Enhancing the Curie Temperature of Ferromagnetic Semiconductor (Ga,Mn)As to 200 K via Nanostructure Engineering. *Nano Lett.* **2011**, *11*, 2584−2589.
(10) Sun, F.; Zhao, G. Q.; Escanhoela, C. A.; Chen, B. J.; Kou, R. H.; Wang, Y. G.; Xiao, Y. M.; Chow, P.; Mao, H. K.; Haskel, D.; Yang, W. G.; Jin, C. Q. Hole doping and pressure effects on the II-II-V-based diluted magnetic semiconductor $(Ba_{1-x}K_x)(Zn_{1-y}Mn_y)_2As_2$. *Phys. Rev. B* **2017**, *95*, No. 094412.
(11) Zhao, G. Q.; Li, Z.; Sun, F.; Yuan, Z.; Chen, B. J.; Yu, S.; Peng, Y.; Deng, Z.; Wang, X. C.; Jin, C. Q. Effects of high pressure on the ferromagnetism and in-plane electrical transport of $(Ba_{0.904}K_{0.096})$-$(Zn_{0.805}Mn_{0.195})_2As_2$ single crystal. *J. Phys.: Condens. Matter* **2018**, *30*, No. 254001.
(12) Suzuki, H.; Zhao, G. Q.; Zhao, K.; Chen, B. J.; Horio, M.; Koshiishi, K.; Xu, J.; Kobayashi, M.; Minohara, M.; Sakai, E.; Horiba, K.; Kumigashira, H.; Gu, B.; Maekawa, S.; Uemura, Y. J.; Jin, C. Q.; Fujimori, A. Fermi surfaces and p−d hybridization in the diluted magnetic semiconductor $Ba_{1-x}K_x(Zn_{1-y}Mn_y)_2As_2$ studied by soft X-ray angle-resolved photoemission spectroscopy. *Phys. Rev. B* **2015**, *92*, No. 235120.
(13) Suzuki, H.; Zhao, K.; Shibata, G.; Takahashi, Y.; Sakamoto, S.; Yoshimatsu, K.; Chen, B. J.; Kumigashira, H.; Chang, F.-H.; Lin, H.-J.; Huang, D. J.; Chen, C. T.; Gu, B.; Maekawa, S.; Uemura, Y. J.; Jin, C. Q.; Fujimori, A. Photoemission and X-ray absorption studies of the isostructural to Fe-based superconductors diluted magnetic semiconductor $Ba_{1-x}K_x(Zn_{1-y}Mn_y)_2As_2$. *Phys. Rev. B* **2015**, *91*, No. 140401(R).
(14) Sun, F.; Li, N. N.; Chen, B. J.; Jia, Y. T.; Zhang, L. J.; Li, W. M.; Zhao, G. Q.; Xing, L. Y.; Fabbris, G.; Wang, Y. G.; Deng, Z.; Uemura, Y. J.; Mao, H. K.; Haskel, D.; Yang, W. G.; Jin, C. Q. Pressure effect on the magnetism of the diluted magnetic semiconductor $(Ba_{1-x}K_x)$-$(Zn_{1-y}Mn_y)_2As_2$ with independent spin and charge doping. *Phys. Rev. B* **2016**, *93*, No. 224403.
(15) Glasbrenner, J. K.; Žutić, I.; Mazin, I. I. Theory of Mn-doped II-II-V semiconductors. *Phys. Rev. B* **2014**, *90*, No. 140403(R).
(16) Yang, J.; Luo, S.; Xiong, Y. First-principles study on the electronic structures and magnetic properties of a diluted magnetic semiconductor $Ba_{1-x}K_x(Zn_{1-y}Mn_y)_2As_2$. *Solid State Sci.* **2015**, *46*, 102−106.

(17) Wang, R.; Huang, Z. X.; Zhao, G. Q.; Yu, S.; Deng, Z.; Jin, C. Q.; Jia, Q. J.; Chen, Y.; Yang, T. Y.; Jiang, X. M.; Cao, L. X. Out-of-plane easy-axis in thin films of diluted magnetic semiconductor $Ba_{1-x}K_x(Zn_{1-y}Mn_y)_2As_2$. *AIP Adv.* **2017**, *7*, No. 045017.
(18) Dieny, B.; Chshiev, M. Perpendicular magnetic anisotropy at transition metal/oxide interfaces and applications. *Rev. Mod. Phys.* **2017**, *89*, No. 025008.
(19) Abolfath, M.; Jungwirth, T.; Brum, J.; MacDonald, A. H. Theory of magnetic anisotropy in $III_{1-x}Mn_xV$ ferromagnets. *Phys. Rev. B* **2001**, *63*, No. 054418.
(20) Dietl, T.; Ohno, H.; Matsukura, F. Hole-mediated ferromagnetism in tetrahedrally coordinated semiconductors. *Phys. Rev. B* **2001**, *63*, No. 195205.
(21) Liu, X.; Sasaki, Y.; Furdyna, J. K. Ferromagnetic resonance in $Ga_{1-x}Mn_xAs$: Effects of magnetic anisotropy. *Phys. Rev. B* **2003**, *67*, No. 205204.
(22) Sawicki, M.; Matsukura, F.; Idziaszek, A.; Dietl, T.; Schott, G. M.; Ruester, C.; Gould, C.; Karczewski, G.; Schmidt, G.; Molenkamp, L. W. Temperature dependent magnetic anisotropy in (Ga,Mn)As layers. *Phys. Rev. B* **2004**, *70*, No. 245325.
(23) Zemen, J.; Kučera, J.; Olejník, K.; Jungwirth, T. Magneto-crystalline anisotropies in (Ga,Mn)As: Systematic theoretical study and comparison with experiment. *Phys. Rev. B* **2009**, *80*, No. 155203.
(24) Stöhr, J.; König, H. Determination of Spin- and Orbital-Moment Anisotropies in Transition Metals by Angle-Dependent X-Ray Magnetic Circular Dichroism. *Phys. Rev. Lett.* **1995**, *75*, 3748−3751.
(25) van der Laan, G.; Chopdekar, R. V.; Suzuki, Y.; Arenholz, E. Strain-Induced Changes in the Electronic Structure of $MnCr_2O_4$ Thin Films Probed by X-Ray Magnetic Circular Dichroism. *Phys. Rev. Lett.* **2010**, *105*, No. 067405.
(26) Mamiya, K.; Koide, T.; Ishida, Y.; Osafune, Y.; Fujimori, A.; Suzuki, Y.; Katayama, T.; Yuasa, S. Angle-resolved soft X-ray magnetic circular dichroism in a monatomic Fe layer facing an MgO(001) tunnel barrier. *Radiat. Phys. Chem.* **2006**, *75*, 1872−1877.
(27) Shibata, G.; Kitamura, M.; Minohara, M.; Yoshimatsu, K.; Kadono, T.; Ishigami, K.; Harano, T.; Takahashi, Y.; Sakamoto, S.; Nonaka, Y.; Keisuke, I.; Zhendong, C.; Mitsuo, F.; Shuichiro, F.; Makoto, O.; Jun-ichi, F.; Akira, U.; Kazunori, W.; Hideyuki, F.; Seiichi, F.; Arata, T.; Hiroshi, K.; Tsuneharu, K.; Atsushi, F. Anisotropic spin-density distribution and magnetic anisotropy of strained $La_{1-x}Sr_xMnO_3$ thin films: angle-dependent X-ray magnetic circular dichroism. *npj Quantum Mater.* **2018**, *3*, 3.
(28) Momma, K.; Izumi, F. VESTA3 for three-dimensional visualization of crystal, volumetric and morphology data. *J. Appl. Crystallogr.* **2011**, *44*, 1272−1276.
(29) Furuse, M.; Okano, M.; Fuchino, S.; Uchida, A.; Fujihira, J.; Fujihira, S.; Kadono, T.; Fujimori, A.; Koide, T. HTS Vector Magnet for Magnetic Circular Dichroism Measurement. *IEEE Trans. Appl. Supercond.* **2013**, *23*, No. 4100704.
(30) Nakajima, R.; Stöhr, J.; Idzerda, Y. U. Electron-yield saturation effects in L-edge X-ray magnetic circular dichroism spectra of Fe, Co, and Ni. *Phys. Rev. B* **1999**, *59*, 6421−6429.
(31) Tanaka, A.; Jo, T. Resonant 3d, 3p and 3s Photoemission in Transition Metal Oxides Predicted at 2p Threshold. *J. Phys. Soc. Jpn.* **1994**, *63*, 2788−2807.
(32) Kobayashi, M.; Niwa, H.; Takeda, Y.; Fujimori, A.; Senba, Y.; Ohashi, H.; Tanaka, A.; Ohya, S.; Hai, P. N.; Tanaka, M.; Harada, Y.; Oshima, M. Electronic Excitations of a Magnetic Impurity State in the Diluted Magnetic Semiconductor (Ga,Mn)As. *Phys. Rev. Lett.* **2014**, *112*, No. 107203.
(33) Gu, B.; Maekawa, S. Diluted magnetic semiconductors with narrow band gaps. *Phys. Rev. B* **2016**, *94*, No. 155202.
(34) Takeda, Y.; Kobayashi, M.; Okane, T.; Ohkochi, T.; Okamoto, J.; Saitoh, Y.; Kobayashi, K.; Yamagami, H.; Fujimori, A.; Tanaka, A.; Okabayashi, J.; Oshima, M.; Ohya, S.; Hai, P. N.; Tanaka, M. Nature of magnetic coupling between Mn Ions in as-grown $Ga_{1-x}Mn_xAs$ studied by X-ray magnetic circular dichroism. *Phys. Rev. Lett.* **2008**, *100*, No. 247202.
(35) Edmonds, K. W.; Farley, N. R. S.; Johal, T. K.; van der Laan, G.; Campion, R. P.; Gallagher, B. L.; Foxon, C. T. Ferromagnetic moment and antiferromagnetic coupling in (Ga,Mn)As thin films. *Phys. Rev. B* **2005**, *71*, No. 064418.
(36) de Groot, F. M. F.; Fuggle, J. C.; Thole, B. T.; Sawatzky, G. A. L_2,3 X-ray-absorption edges of d^0 compounds: K^+, Ca^{2+}, Sc^{3+}, and Ti^{4+} in O_h (octahedral) symmetry. *Phys. Rev. B* **1990**, *41*, 928−937.
(37) Teramura, Y.; Tanaka, A.; Jo, T. Effect of Coulomb Interaction on the X-Ray Magnetic Circular Dichroism Spin Sum Rule in 3 d Transition Elements. *J. Phys. Soc. Jpn.* **1996**, *65*, 1053−1055.
(38) Takeda, Y.; Ohya, S.; Pham, N. H.; Kobayashi, M.; Saitoh, Y.; Yamagami, H.; Tanaka, M.; Fujimori, A. Direct observation of the magnetic ordering process in the ferromagnetic semiconductor $Ga_{1-x}Mn_xAs$ via soft X-ray magnetic circular dichroism. *J. Appl. Phys.* **2020**, *128*, No. 213902.
(39) Sakamoto, S.; Anh, L. D.; Hai, P. N.; Shibata, G.; Takeda, Y.; Kobayashi, M.; Takahashi, Y.; Koide, T.; Tanaka, M.; Fujimori, A. Magnetization process of the *n*-type ferromagnetic semiconductor (In,Fe)As:Be studied by X-ray magnetic circular dichroism. *Phys. Rev. B* **2016**, *93*, No. 035203.
(40) Sakamoto, S.; Anh, L. D.; Hai, P. N.; Takeda, Y.; Kobayashi, M.; Wakabayashi, Y. K.; Nonaka, Y.; Ikeda, K.; Chi, Z.; Wan, Y.; Suzuki, M.; Saitoh, Y.; Yamagami, H.; Tanaka, M.; Fujimori, A. Magnetization process of the insulating ferromagnetic semiconductor (Al,Fe)Sb. *Phys. Rev. B* **2020**, *101*, No. 075204.
(41) Yang, H. X.; Chshiev, M.; Dieny, B.; Lee, J. H.; Manchon, A.; Shin, K. H. First-principles investigation of the very large perpendicular magnetic anisotropy at Fe|MgO and Co|MgO interfaces. *Phys. Rev. B* **2011**, *84*, No. 054401.
(42) Okabayashi, J.; Koo, J. W.; Sukegawa, H.; Mitani, S.; Takagi, Y.; Yokoyama, T. Perpendicular magnetic anisotropy at the interface between ultrathin Fe film and MgO studied by angular-dependent X-ray magnetic circular dichroism. *Appl. Phys. Lett.* **2014**, *105*, No. 122408.
(43) Nakajima, N.; Koide, T.; Shidara, T.; Miyauchi, H.; Fukutani, H.; Fujimori, A.; Iio, K.; Katayama, T.; Nývlt, M.; Suzuki, Y. Perpendicular Magnetic Anisotropy Caused by Interfacial Hybridization via Enhanced Orbital Moment in Co/Pt Multilayers: Magnetic Circular X-Ray Dichroism Study. *Phys. Rev. Lett.* **1998**, *81*, 5229−5232.

https://dx.doi.org/10.1021/acsaelm.0c00938
ACS Appl. Electron. Mater. 2021, 3, 789−794